www.nature.com/aps

Acta Pharmacologica Sinica

ARTICLE

Protein tyrosine phosphatase L1 represses endothelial-mesenchymal transition by inhibiting IL-1β/NF-κB/Snail signaling

Xiao-min Wei[1], Gulinuer Wumaier[1], Ning Zhu[1], Liang Dong[1], Cheng-wei Li[1], Jing-wen Xia[1], You-zhi Zhang[1], Peng Zhang[1], Xiu-juan Zhang[1], Yuan-yuan Zhang[1] and Sheng-qing Li[1]

Endothelial–mesenchymal transition (EnMT) plays a pivotal role in various diseases, including pulmonary hypertension (PH), and transcription factors like Snail are key regulators of EnMT. In this study we investigated how these factors were regulated by PH risk factors (e.g. inflammation and hypoxia) in human umbilical vein endothelial cells (HUVECs). We showed that treatment with interleukin 1β (IL-1β) induced EnMT of HUVECs via activation of NF-κB/Snail pathway, which was further exacerbated by knockdown of protein tyrosine phosphatase L1 (PTPL1). We demonstrated that PTPL1 inhibited NF-κB/Snail through dephosphorylating and stabilizing IκBα. IL-1β or hypoxia could downregulate PTPL1 expression in HUVECs. The deregulation of PTPL1/NF-κB signaling was validated in a monocrotaline-induced rat PH (MCT-PH) model and clinical PH specimens. Our findings provide novel insights into the regulatory mechanisms of EnMT, and have implications for identifying new therapeutic targets for clinical PH.

Keywords: pulmonary hypertension; endothelial–mesenchymal transition (EnMT); NF-κB; protein tyrosine phosphatase L1 (PTPL1); human umbilical vein endothelial cells (HUVECs)

Acta Pharmacologica Sinica (2020) 41:1102–1110; https://doi.org/10.1038/s41401-020-0374-x

INTRODUCTION

Endothelial–mesenchymal transition (EnMT) is a cellular process characterized by the loss of endothelial features and the acquisition of mesenchymal, fibroblast, or stem-cell-like characteristics [1]. It is defined by the loss of cellular adhesion and the cytoskeletal reorganization of actin and intermediate filaments that convert apical–basal polarity to front end–back end polarity to form spindle-shaped cells. During this transformation, there is a marked decrease in endothelial biomarkers such as CD144 and CD31, as well as increased expression of mesenchymal biomarkers such as α-SMA and SM-22α [2]. EnMT plays a pivotal role in various pathologic conditions, such as atherosclerosis [3], tumors [4, 5], vein graft failure [6], and fibrosis in key organs [7–9]. A recent study has shown that abnormal differentiation of EnMT-derived SM-like cells results in pulmonary hypertension (PH) [10–12]. However, the underlying mechanism remains to be fully elucidated.

Inflammation and hypoxia contribute to the pathogenesis of various types of PH, especially group III PH. Expression of nuclear factor-κB (NF-κB) and the pro-inflammatory cytokine interleukin-1β (IL-1β) is elevated in the lung tissue of a rat model of monocrotaline-induced PH (MCT-PH), and NF-κB activation may contribute to the development of this condition [13]. IL-1β could induce EnMT by activating the NF-κB pathway [14]. The NF-κB-regulated gene Snail is a key regulator of EnMT, cell adhesion, and proliferation [15, 16]. These findings highlight the critical role of NF-κB/Snail signaling in EnMT.

Protein tyrosine phosphatase L1 (PTPL1) is a high-molecular-weight (270 kDa) nonreceptor-type phosphatase. It contains multiple domains, providing numerous potential interfaces [17]. Previous studies have shown that PTPL1 plays an important role in the development of tumors [18–20] and idiopathic pulmonary fibrosis [21]. Recent studies have also shown that PTPL1 inhibits EMT in hepatocellular carcinoma [22]. However, the regulatory role and underlying molecular mechanisms of PTPL1 in PH, a disorder attributed necessarily to EnMT of vascular endothelial cells, are not clearly elucidated. Here, we investigated the role of PTPL1 in IL-1β-induced EnMT using human umbilical vein endothelial cells (HUVECs). Our findings suggest that PTPL1 represses EnMT by stabilizing IκBα, and therefore inhibiting the IL-1β/NF-κB/Snail pathway. It may help identify new potential drug targets for PH.

MATERIALS AND METHODS

A rat model of MCT-PH

Adult male Sprague-Dawley rats weighing 150–200 g were purchased from Shanghai SLAC Laboratory Animal Co. Ltd (Shanghai, China). All animal studies were approved by the Ethics Committee of Experimental Research at Fudan University Shanghai Medical College and were in accordance with the Institutional Animal Care and Use Committee Guidelines.

Animals were randomly divided into two groups ($n = 8$/group). The control group rats received phosphate-buffered saline (PBS).

[1]Department of Pulmonary and Critical Care Medicine, Huashan Hospital, Fudan University, Shanghai 200040, China
Correspondence: Sheng-qing Li (shengqingli@hotmail.com)
These authors contributed equally: Xiao-min Wei, Gulinuer Wumaier

Received: 18 August 2019 Accepted: 4 February 2020
Published online: 9 March 2020

The MCT group rats received MCT (60 mg/kg; Sigma, St. Louis, MO, USA). All animals were raised under a 12 h:12 h light–dark cycle and were freely supplied with food and water. The room temperature was maintained at 25 °C, and the bedding was changed once per week.

Hemodynamic analysis and tissue preparation
In the rat model of MCT-PH, rat pulmonary vascular and hemodynamic alterations and RV remodeling occurred 28 days after MCT injection. At that point, the right jugular vein was carefully isolated. A specially shaped catheter linked to the PowerLab system (AD Instruments, Bella Vista, NSW, Australia) was inserted into the right ventricle (RV) via this vein, and right ventricular systolic pressure (RVSP) was recorded. Then, sternotomy was performed, and rats were perfused with paraformaldehyde. Both lungs and the heart were harvested. The RV and the left ventricle plus septum (LV + S) were weighed, and the RV/LV + S weight ratio was determined as an indication of right ventricular hypertrophy. Next, the lower lobe of the right lung was sectioned into 4-mm-thick slices and soaked in a 10% formalin solution (pH 7.4). The other parts were kept at −80 °C for further experiments.

Hematoxylin and eosin staining
The fixed lungs were sliced in the mid-sagittal plane, embedded in paraffin, and cut into ~5-μm-thick sections with a microtome. Then, the sections were placed on glass slides, stained with hematoxylin and eosin (HE) for morphological analysis, and visualized under an Olympus BX41 microscope (Tokyo, Japan).

Cell culture and induction of EnMT
HUVECs (passages 3–5; ScienCell Research Laboratories, California, USA) were cultured in endothelial cell medium (ECM). To induce EnMT, recombinant IL-1β (10 ng/mL; Peprotech) in 0.5% fetal bovine serum medium was used to treat the cells for 48 h. Human Pulmonary Artery Endothelial Cells (HPAECs) (passages 3–5; ScienCell Research Laboratories, California, USA) were cultured in ECM. Cells were maintained in a humidified atmosphere at 37 °C in 5% CO_2.

Immunofluorescence staining
Cells were fixed with 4% paraformaldehyde for 30 min at room temperature. The cells were then incubated with primary antibodies against α-SMA and CD31 (Abcam, Cambridge, MA, USA) overnight at 4 °C and subsequently with Alexa Fluor-conjugated secondary antibodies (Invitrogen, Carlsbad, CA) for 2 h at 37 °C. After nucleus staining with 4′,6-diamidino-2-phenylindole (DAPI) dye, cells were examined under a fluorescence microscope. A minimum of three replicates were performed for each examination.

Lentiviral construction and transduction
The lentiviral shuttle vector for the PTPL1-targeted short hairpin RNA, sh-PTPL1, and the packaging vectors, including pMD2.0G and psPAX, were purchased from Addgene (Cambridge, MA, USA). They were transfected into HEK293T cells for packaging and amplification of lentivirus. For transient transduction, cells at approximately 80% confluence were transduced with the lentiviral vectors at a multiplicity of infection of 60 for 4 h. Afterward, the media were changed to fresh ECM, and the transfected cells were cultured for an additional 72 h.

Quantitative RT-PCR
Total RNA was extracted from cultured cells using TRIzol reagent (Invitrogen, Life Technologies, Carlsbad, CA, USA). Reverse transcription was performed using a first-strand cDNA reverse transcription kit (Takara, Otsu, Japan), and real-time PCR was performed using a SYBR Green/ROX qPCR Master Mix kit according to the manufacturer's instructions (Takara, Otsu, Japan). The relative quantification was determined using the ΔΔCt method with β-actin as a reference gene. All primer sequences are shown in Table 1.

Western blotting
Proteins from cultured cells were extracted with radioimmunoprecipitation assay lysis buffer and quantified with the bicinchoninic acid protein assay kit. Then, the proteins were separated with sodium dodecyl sulfate-polyacrylamide gel electrophoresis (SDS-PAGE) and transferred to a polyvinylidene fluoride transfer membrane. The membranes were blocked in 5% nonfat dry milk for 1 h, followed by incubation overnight at 4 °C with primary antibodies. The membranes were then washed and incubated with secondary antibodies, washed with Tris-buffered saline and Tween 20 (0.1%), and treated with electrochemiluminescence reagents for blot detection. Blots were quantified by densitometry using ImageJ (NIH Image, Bethesda, MD). The primary antibodies used are as follows: CD31 (1:1000), α-SMA (1:100), CD144 (1:1000), SM-22α (1:1000), IκBα (1:1000), phospho-IκBα (Y42, 1:1000), and β-actin (1:1000) were purchased from Abcam (Cambridge, MA, USA); PTPL1 (1:1000) was purchased from Novus Biologicals; and NF-κB (1:1000), phospho-NF-κB (p65, 1:1000), and Snail (1:1000) were purchased from Cell Signaling Technology (Danvers, MA, USA). Secondary horseradish-peroxidase-conjugated antibodies were purchased from Jackson ImmunoResearch Laboratories (1:5000, dilution; ImmunoResearch Laboratories, Inc., West Grove, PA, USA).

Immunohistochemical assay
All the specimens were fixed with 4% paraformaldehyde and embedded with paraffin. Four-micrometer-thick sections were cut and transferred to glass slides coated with 100 g/L polylysine. The immunohistochemical (IHC) staining was performed as described

Table 1. Primers used for qPCR

Gene	Forward 5′–3′	Reverse 5′–3′
CD31 (Human)	ACCAGAGCTATTCCCAAAAGACC	TGCGGCGATTCATCAGGAAAT
CD144 (Human)	AGAGCTCCACTCACGCTCAG	CATCTTCCCAGGAGGAACAG
α-SMA (Human)	AAGCACAGAGCAAAAGAGGAAT	ATGTCGTCCCAGTTGGTGAT
SM-22α (Human)	AGTGCAGTCCAAAATCGAGAAG	CTTGCTCAGAATCACGCCAT
PTPL1 (Human)	TGGCTCTCCAGGCTGAGTATG	AACACCAAACAAAATGGTCCTG
β-actin (Human)	GGACCTGACTGACTACCTCAT	CGTAGCACAGCTTCTCCTTAAT
IL-1β (Rat)	TTCAGCAGTAAAGCGTGTGG	GCGTGTGTGTGTGTGTGTGT
IL-6 (Rat)	ACCACCCACAACAGACCAGT	TTTCACAGCCTACCCACCTC
TNF-α (Rat)	AGAGCCCCCAATCTGTGTC	TTCAGCGTCTCGTGTGTTTC
PTPL1 (Rat)	TGACACACCATGGTCACAGTT	CGACAGAAGTAGCATCGCCG
GAPDH (Rat)	CCATTCTTCCACCTTTGATGCT	TGTTGCTGTAGCCATATTCATTGT

[23]. Anti-PTPL1 antibody was purchased from Novus Biologicals. The primary antibodies were diluted in PBS (1:50). IHC was also performed on paraffin-embedded sections. The sections were autoclaved for 10 min at 121 °C for antigen retrieval. An Envision kit (DAKO, Glostrup, Denmark) was used for staining according to the manufacturer's instructions.

Immunoprecipitation

Cells were lysed in buffer containing 1% (v/v) Nonidet P-40, 0.5 mM EGTA, 5 mM sodium orthovanadate, 10% (v/v) glycerol, 100 μg/mL phenylmethylsulfonyl fluoride, 1 μg/mL leupeptin, 1 μg/mL pepstatin A, 1 μg/mL aprotinin, and 50 mM HEPES (pH 7.5). Thereafter, 1000 μL of diluted lysate (1 μg protein/μL) was incubated overnight with 5 μg of an antibody for immunoprecipitation (IP). Immune complexes were captured by adding 40 μL of a 1:1 (v/v) suspension of protein A:Sepharose 4B beads and rotating the mixture for 2 h at 4 °C. The beads were harvested, and the bound proteins were resolved by SDS-PAGE and analyzed by Western blotting. The primary antibodies used for IP are described in the Western blotting section.

Migration assays

Cell migration was assessed using transwell chambers (24 wells, 8 μm pore size; BD Biosciences, San Diego, CA, USA). Samples containing 1×10^5 cells were resuspended in serum-free ECM and loaded into the upper chamber. The chambers were incubated for 24 h, with complete culture medium added to the lower chamber. Nonmobile cells were removed, and the chambers were stained with crystal violet. Five randomly selected fields were counted under an inverted light microscope.

Tube formation assays

HUVECs were harvested and suspended in ECM. Forty-eight-well plates were coated with Matrigel (BD Biosciences), which was allowed to polymerize at 37 °C in a 5% CO_2 chamber for 30 min. HUVECs (1×10^4 cells/mL) were added to each chamber, treated as indicated, and incubated for 8 h at 37 °C in 5% CO_2, followed by observation of capillary-like tube formation using phase-contrast microscopy.

RNA-Seq analysis

We analyzed the change in the mRNA profiles between HPAECs that were treated with and without hypoxia for 6 h. Total RNA was isolated using TRIzol reagent (Invitrogen, Carlsbad, CA, USA) according to the manufacturer's instructions. cDNA library preparation was performed using the RNA-Seq Sample Prep Kit (Illumina, NEB, Ipswich, MA, USA) according to the manufacturer's instructions. For the QC step, an Agilent 2100 Bioanalyzer and an ABI StepOnePlus Real-Time PCR System were used to qualify and quantify the sample library. Each cDNA library was amplified once before sequencing. Sequencing was performed on an Illumina HiSeq X Ten at Biotecan Co., Ltd sequencer (Shanghai, China). The RNA-Seq data were analyzed as previously described [24, 25]. Differentially expressed genes (with a fold change over 1.5 and $P < 0.05$) were selected.

Statistical analysis

Data are presented as the means ± SEMs. All experiments were repeated at least three times. Statistical analysis was performed with GraphPad Prism 7.0 software. Comparisons among groups were made using one-way analysis of variance or Student's *t*-test. *P* values <0.05 were considered significant.

RESULTS

IL-1β induces EnMT in HUVECs by activating the NF-κB/Snail pathway

Exposure of HUVECs to IL-1β (10 ng/mL) for 48 h caused an obvious alteration in cellular morphology from a polygonal, cobblestone-like shape to a more spindle and fibroblast-like shape (Fig. 1a). Quantitative RT-PCR (qRT-PCR) showed that IL-1β treatment reduced the mRNA levels of endothelial markers (CD31 and CD144 were greatly reduced) and increased those of the mesenchymal markers α-SMA and SM-22α (Fig. 1b). To further confirm that EnMT was induced by IL-1β, the protein levels of the endothelial or mesenchymal markers were examined by Western blot assay and immunofluorescent staining. As a result, CD31 and CD144 were significantly downregulated, and α-SMA and SM-22α were remarkably upregulated by IL-1β treatment (Fig. 1c, d). In addition, HUVEC tube formation was significantly inhibited by IL-1β (Fig. 1e). Consistent with the transition to a mesenchymal phenotype, HUVECs treated with IL-1β exhibited enhanced migration capabilities when compared with untreated cells (Fig. 1f). Exposure of HUVECs to IL-1β activated NF-κB signaling and increased the level of Snail (Fig. 1g). These results suggest that IL-1β likely elicits EnMT of HUVECs via NF-κB/Snail signaling.

PTPL1 impairs IL-1β-induced EnMT by inactivating NF-κB

We next examined the regulatory role of PTPL1 in the IL-1β-induced EnMT of HUVECs. PTPL1 was knocked down in HUVECs via lentiviral vector-based sh-RNAs (Fig. 2a–c). Consequently, PTPL1 knockdown increased the mRNA and protein expression of α-SMA and SM-22α and decreased CD31 and CD144 expression (Fig. 2d, e). The HUVEC tube formation capacity was significantly inhibited after PTPL1 silencing (Fig. 2f). In accordance with the transition to a mesenchymal phenotype, PTPL1-knockdown HUVECs displayed enhanced migration abilities compared with the control cells (Fig. 2g). Control and PTPL1-knockdown HUVECs were further subjected to treatment with IL-1β (10 ng/mL) for 48 h. We found that knockdown of PTPL1 synergized with IL-1β to upregulate the mesenchymal proteins α-SMA and SM-22α and impair the expression of the endothelial biomarkers CD31 and CD144 (Fig. 2h). Similarly, PTPL1-knockdown HUVECs showed much higher NF-κB activity and Snail levels than control cells in response to treatment with IL-1β (Fig. 2i). These data indicate that PTPL1 represses the IL-1β-induced EnMT of HUVECs by counteracting NF-κB/Snail signaling.

PTPL1 inhibits the NF-κB signaling pathway by stabilizing IκBα

PTPL1 has been predicted to dephosphorylate various proteins, including IκBα [26]. We thus investigated whether PTPL1 inhibits NF-κB activity and impedes the EnMT of HUVECs by targeting IκBα. Indeed, PTPL1 was coimmunoprecipitated with IκBα from HUVEC lysates (Fig. 3a). While IL-1β induced the phosphorylation of IκBα at tyrosine 42 and triggered its degradation in HUVECs, PTPL1 knockdown further promoted the phosphorylation and downregulation of the IκBα protein (Fig. 3b). Therefore, PTPL1 may attenuate NF-κB signaling by dephosphorylating IκBα and increasing its half-life in vascular endothelial cells.

PTPL1 is downregulated by IL-1β and hypoxia in human vascular endothelial cells

We next asked how the expression of PTPL1 was regulated in vascular endothelial cells. We found that treatment of HUVECs with IL-1β significantly reduced the levels of PTPL1 (Fig. 4a, b). Tissue hypoxia is a risk factor for diverse clinical disorders, e.g., group 3 PH, that pathologically involves EMT [27, 28] or EnMT [29–31]. We thus probed whether hypoxia plays a regulatory role in PTPL1 expression in vascular endothelial cells. Our RNA-Seq results showed that hypoxia treatment of HPAECs induced robust changes in the expression profile of genes, including PTPL1 (Fig. 4c). The downregulation of PTPL1 by hypoxia in HUVECs was further verified by Western blot (Fig. 4d). These results show that PTPL1 downregulation by inflammatory factors or hypoxia contributes to the EnMT of vascular endothelial cells.

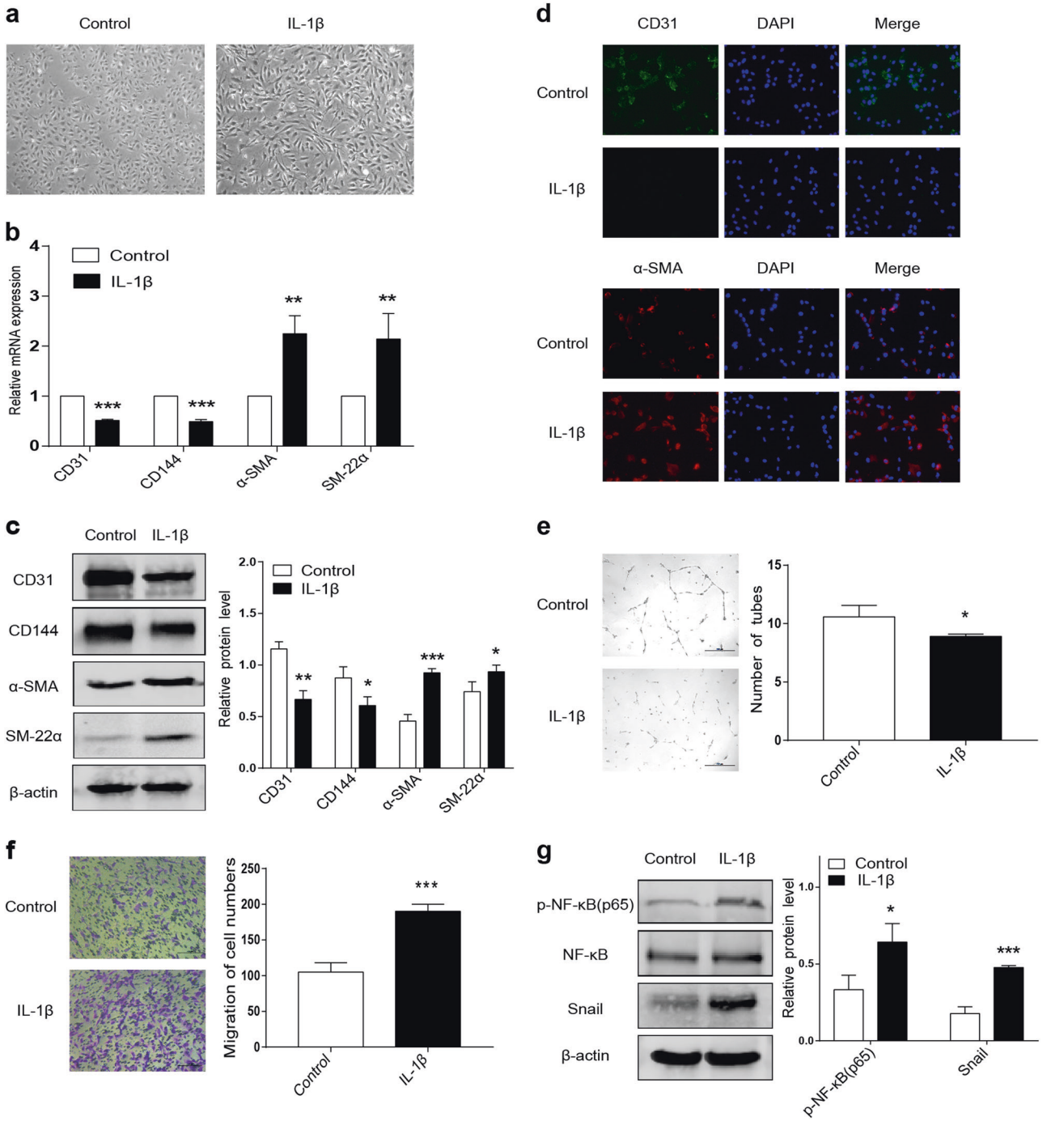

Fig. 1 IL-1β induces EnMT in HUVECs by activating the NF-κB/Snail pathway. **a** Microscopy of HUVECs treated with or without IL-1β (10 ng/mL) for 48 h. IL-1β-treated HUVECs had a fibroblast-like phenotype, whereas untreated control cells had an endothelial cell phenotype. **b** The relative mRNA levels of the endothelial markers CD31 and CD144 and the mesenchymal markers α-SMA and SM-22-α in control and IL-1β-treated HUVECs were assessed by qRT-PCR (each bar represents the mean ± SEM. $^{**}P < 0.01$, $^{***}P < 0.001$ vs. the control group). **c** The protein levels of CD31, CD144, α-SMA, and SM-22-α in control and IL-1β-treated HUVECs were determined by Western blot analysis. (each bar represents the mean ± SEM. $^{*}P < 0.05$, $^{**}P < 0.01$, $^{***}P < 0.001$ vs. the control group). **d** Immunofluorescent staining of CD31 (green) and α-SMA (red) expression in control and IL-1β-treated HUVECs. **e** Tube formation assays for unstimulated and IL-1β-exposed HUVECs (each bar represents the mean ± SEM. $^{*}P < 0.05$ vs. the control group). **f** Transwell assay to assess the migration of unstimulated and IL-1β-exposed HUVECs (wach bar represents the mean ± SEM. $^{***}P < 0.001$ vs. the control group). **g** The protein levels of p-NF-κB (p65), NF-κB, and Snail were determined by Western blot analysis using lysates from unstimulated and IL-1β-exposed HUVECs (each bar represents the mean ± SEM. $^{*}P < 0.05$, $^{***}P < 0.001$ vs. the control group)

PTPL1/NF-κB signaling participates in PH pathogenesis

We evaluated the involvement of PTPL1 and the NF-κB pathway in the pathogenesis of PH. A rat model of MCT-induced PH (MCT-PH) was established via exposure to MCT for 4 weeks, as verified by significantly increased RVSP (Fig. 5a) and mean pulmonary arterial pressure (mPAP) (Fig. 5b) and a significantly increased ratio of right ventricle to left ventricle plus septum (RV/LV + S) weight (Fig. 5c). To validate NF-κB activation in vivo,

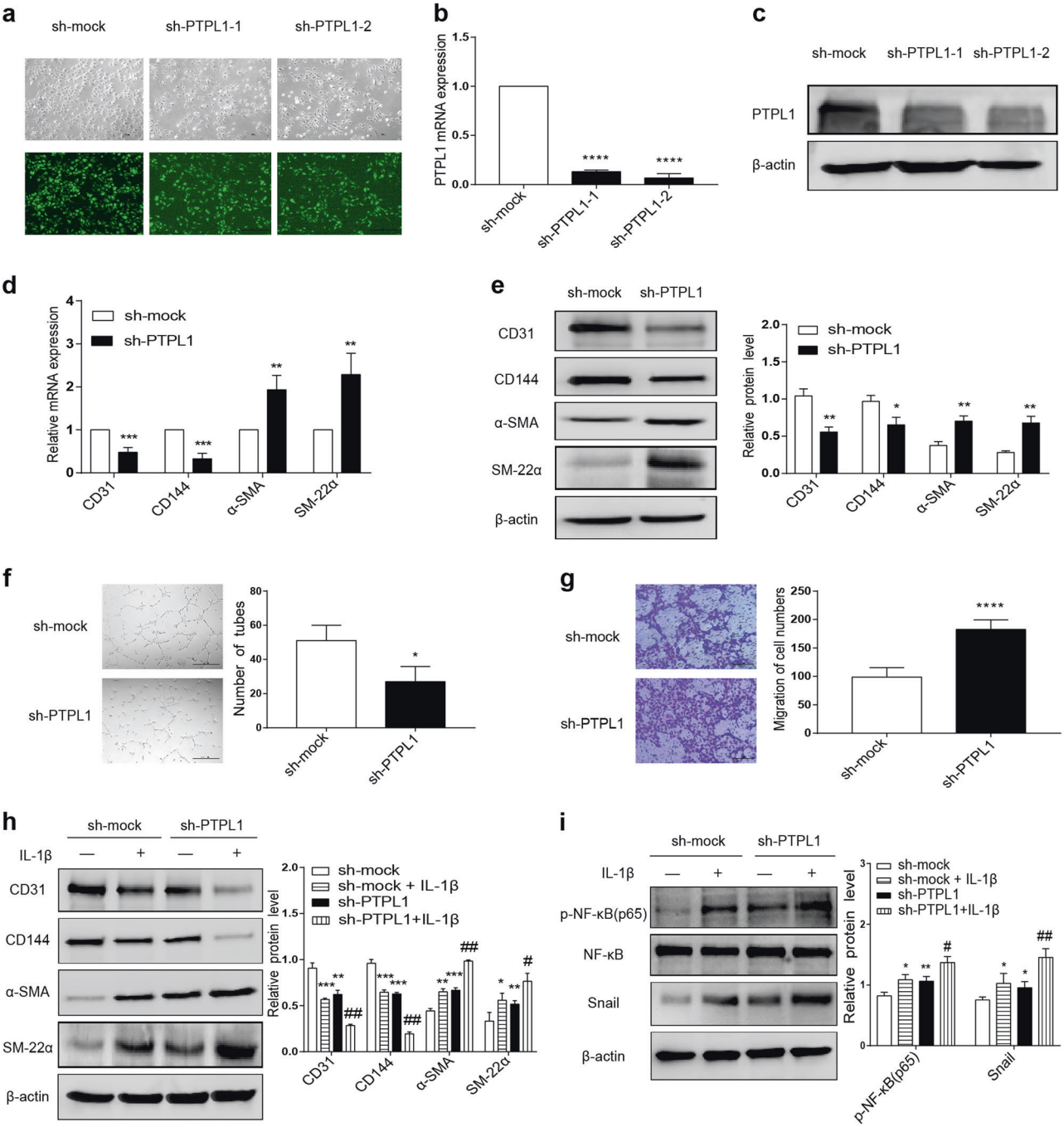

Fig. 2 PTPL1 impairs IL-1β-induced EnMT by inactivating NF-κB. **a** Fluorescent microscopy of HUVECs infected with recombinant lentiviruses expressing control or PTPL1-targeted sh-RNA for 72 h. **b–e** The PTPL1 levels in cells in **a** were measured by qRT-PCR (**b**, **d**) and Western blot (**c**, **e**) (each bar represents the mean ± SEM. $^{*}P < 0.05$, $^{**}P < 0.01$, $^{***}P < 0.001$, $^{****}P < 0.0001$ vs. the sh-mock group). **f** Tube formation assay for cells in **a** (each bar represents the mean ± SEM. $^{*}P < 0.05$ vs. the sh-mock group). **g** Cell migration was assessed by transwell assays (each bar represents the mean ± SEM. $^{****}P < 0.0001$ vs. the sh-mock group). **h**, **i** The cells in **a** were treated with IL-1β (10 ng/mL) and were subjected to Western blot analysis (each bar represents the mean ± SEM. $^{*}P < 0.05$, $^{**}P < 0.01$, $^{***}P < 0.001$ vs. the sh-mock group; $^{\#}P < 0.05$, $^{\#\#}P < 0.01$ vs. the sh-PTPL1 group)

we generated a rat model of MCT-PH characterized by abnormal media thickening (Fig. 5d). Quantitative RT-PCR showed that the expression of pro-inflammatory cytokines, such as tumor necrosis factor-α (TNF-α), interleukin (IL)-6 and interleukin (IL)-1β, was increased, whereas the level of PTPL1 was reduced in the lung tissue of MCT-PH rats compared to control rats (Fig. 5e, f). We also found that the level of phosphorylated NF-κB protein was significantly elevated in the lung tissue of MCT-PH rats compared to control rats (Fig. 5g). In addition, we collected lung tissue samples from five patients with PH and examined the expression of PTPL1 in the lung tissues of different patients by immunohistochemical staining. The results showed that PTPL1 levels were lower in the pulmonary arterial endothelial cells of PH patients than in control lung cancer patients (Fig. 5h). Therefore, PTPL1 might suppress the development of PH via inhibition of NF-κB activity.

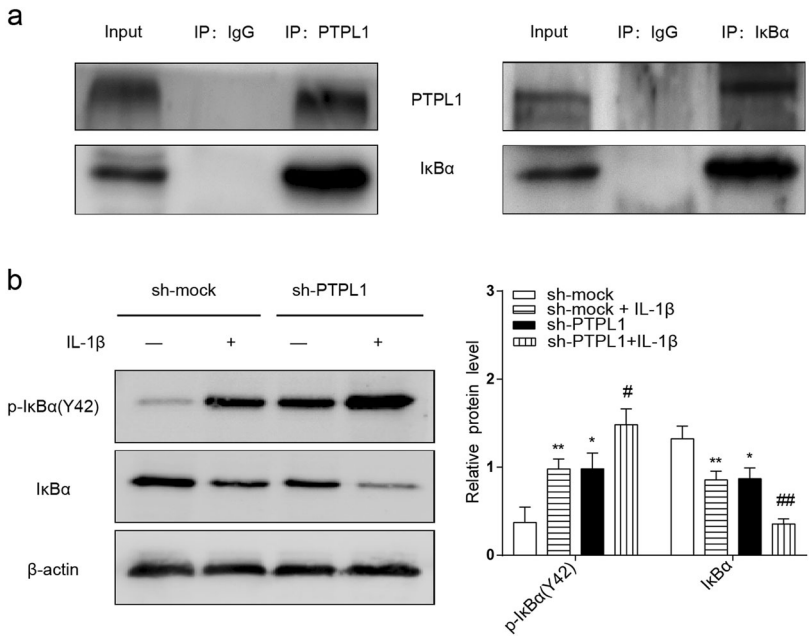

Fig. 3 PTPL1 inhibits the NF-κB signaling pathway by stabilizing IκBα. **a** Immunoprecipitation of PTPL1 and IκBα using lysates from HUVECs. **b** HUVECs infected with sh-mock or sh-PTPL1 lentiviruses were further treated with IL-1β (10 ng/mL) and were subjected to Western blot analysis (each bar represents the mean ± SEM. $^{*}P < 0.05$, $^{**}P < 0.01$ vs. the sh-mock group; $^{\#}P < 0.05$, $^{\#\#}P < 0.01$ vs. the sh-PTPL1 group)

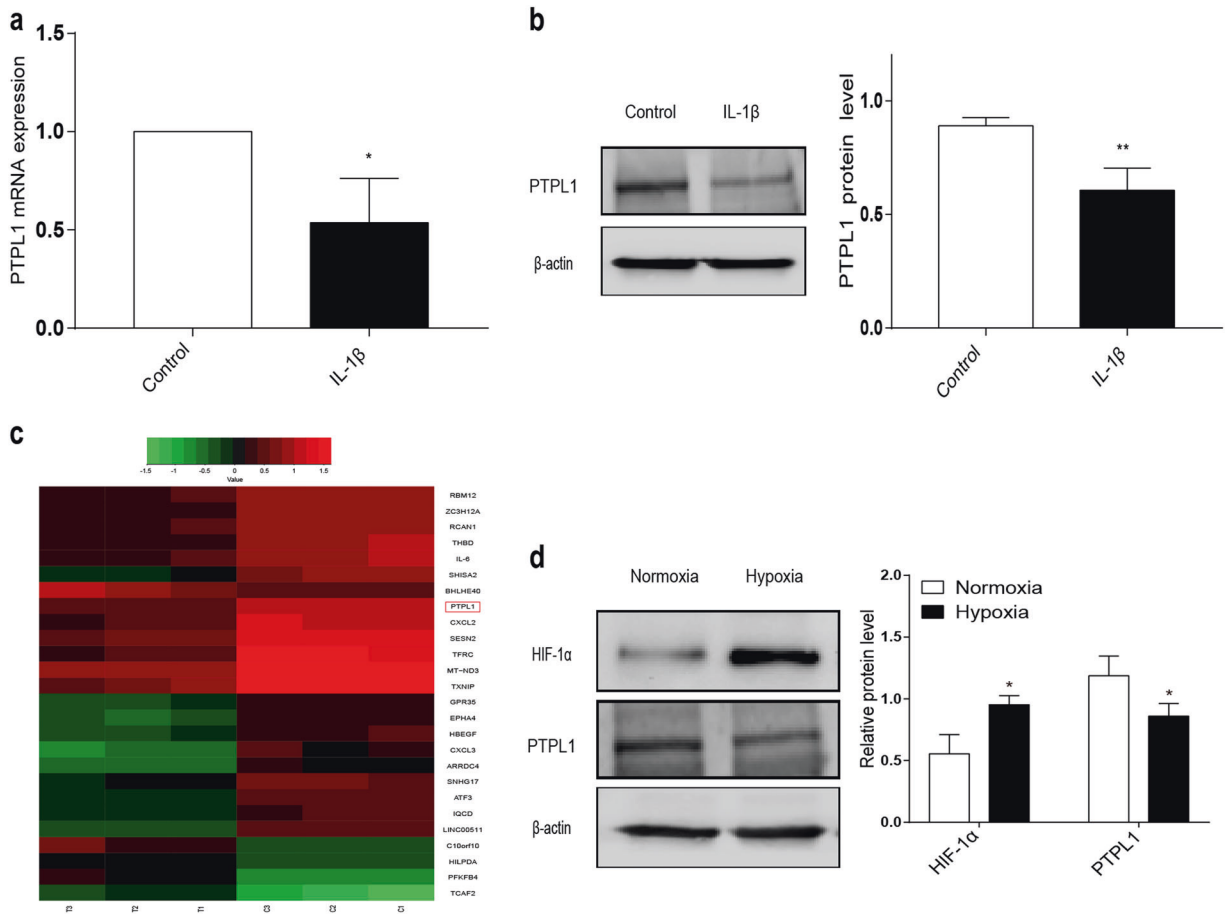

Fig. 4 PTPL1 is downregulated by IL-1β and hypoxia in human vascular endothelial cells. **a**, **b** HUVECs were treated with IL-1β (10 ng/mL) for 48 h and subjected to qRT-PCR (**a**) and Western blot analysis (**b**) (each bar represents the mean ± SEM. $^{*}P < 0.05$, $^{**}P < 0.01$ vs. the control group). **c** Heatmap of RNA-Seq data in HPAECs after hypoxia treatment (T: hypoxia; C: normoxia). **d** Western blot analysis of HUVECs exposed to hypoxia (1% O_2, 94% N_2, and 5% CO_2) for 48 h (each bar represents the mean ± SEM. $^{*}P < 0.05$ vs. the normoxia group)

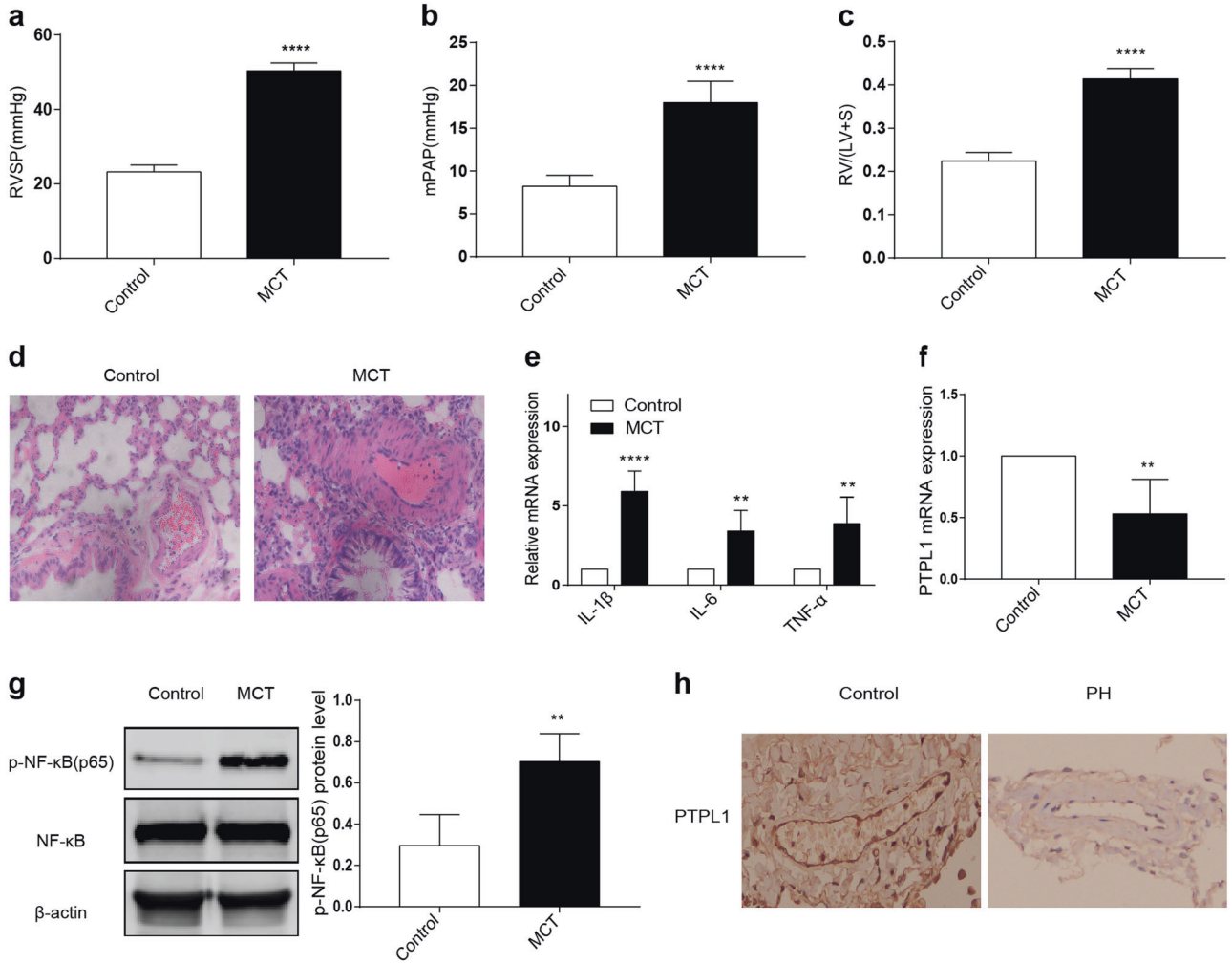

Fig. 5 PTPL1/NF-κB signaling is involved in in vivo PH pathogenesis. **a–c** Rats were treated with MCT as described in the Materials and methods. RVSP (**a**), mPAP (**b**), and RV/(LV + S) (**c**) data were obtained from each group and plotted (each bar represents the mean ± SEM. $^{****}P < 0.0001$ vs. the control group). **d** HE staining of paraffin-fixed lung sections for morphological analysis of pulmonary arteries from control or MCT-PH rats. **e–g** Pulmonary artery samples from control or MCT-PH rats were used for qRT-PCR (**e**, **f**) and Western blot (**g**) analyses. **h** Immunohistochemical staining of lung tissues from PH patients and control lung cancer patients. Bar, 50 μm (each bar represents the mean ± SEM. $^{**}P < 0.01$, $^{****}P < 0.0001$. vs. the control group)

DISCUSSION

In this study, we demonstrated that PTPL1 suppresses the IL-1β-induced EnMT process in HUVECs by impairing NF-κB/Snail signaling. It has been established that EnMT plays critical roles in PH [23, 32, 33]. IL-1β is one of the most important pro-inflammatory cytokines that elicit EnMT [34–36]. We found that HUVECs exposed to IL-1β could undergo EnMT, as verified by the transition of cells to a spindle-like shape, varied expression of endothelial and fibroblast markers, increased migration ability, and reduced tube formation capacity. Consistent with studies reporting that the NF-κB/Snail pathway plays an important role in EMT [37, 38], we found that IL-1β induced EnMT in HUVECs through activation of NF-κB and upregulation of Snail. The activity of NF-κB is regulated by divergent stimuli dependent upon the intracellular signaling context [39, 40], which prompted us to explore the regulatory mechanisms of NF-κB activation in the inflammatory factor-induced EnMT of vascular endothelial cells.

PTPL1 is a nonreceptor-type protein tyrosine phosphatase involved in various cellular signal pathways. Previous studies have found that PTPL1 acts as both a tumor promoter [41] and a suppressor [42]. A previous study showed that PTPL1 over-expression significantly inhibited the progression of hepatocellular carcinoma cells by inhibiting EMT [22]. In this study, we found that PTPL1 could inhibit IL-1β-induced EnMT in HUVECs, and knock-down of PTPL1 could activate NF-κB signaling and increase the level of Snail. Unlike previous studies showing that PTPL1 controls NF-κB activation via p75NTR [43], we found that PTPL1 attenuates NF-κB activation by dephosphorylating IκBα at tyrosine 42 and consequently increasing the half-life of IκBα. These findings are in agreement with a recent report that PTPL1 could target IκBα in ovarian cancer cells [44]. Nonetheless, given the wide crosstalk between intracellular signaling pathways and the relatively low number of protein tyrosine phosphatases compared with protein tyrosine kinases, we cannot rule out that PTPL1 also regulates EnMT by targeting other pathways in vascular endothelial cells.

Both inflammation [45–47] and hypoxia [48, 49] contribute to the pathogenesis of various forms of PH. Our study showed that hypoxia or IL-1β could downregulate PTPL1 in vascular endothelial cells, consistent with a previous finding that PTPL1 expression was impeded upon exposure of prostate cancer cells to hypoxia [50]. We also found that the expression of inflammatory cytokines such as TNF-α, IL-6, and IL-1β was increased in the lung tissue of a rat model of MCT-PH, adding weight to the probability that the inflammatory microenvironment and endothelial PTPL1 in the

lung form a feedback circuit to control EnMT and the pathogenesis of PH. Together, the present findings demonstrated a suppressive role of PTPL1 in EnMT and the deregulation of PTPL1/NF-κB signaling in the pathogenesis of PH.

ACKNOWLEDGEMENTS

This work was supported by the National Natural Science Foundation of China (Nos. 81670045, 81272586, 81470249, and 81970048) and the Chinese Postdoctoral Science Foundation (No. 2014M560759). We are grateful for the financial support from the National Natural Science Foundation (No. 81670045, 81272586, 81470249, 81970048).

AUTHOR CONTRIBUTIONS

SQL designed the experiments and prepared the initial manuscript. XMW and GW conducted the experiments. LD and NZ cultivated the cells. CWL and JWX were responsible for the experimental calculations. YZZ, XJZ, YYZ, and PZ were involved in the experimental analysis.

ADDITIONAL INFORMATION

Competing interests: The authors declare no competing interests.

REFERENCES

1. Kovacic JC, Mercader N, Torres M, Boehm M, Fuster V. Epithelial-to-mesenchymal and endothelial-to-mesenchymal transition: from cardiovascular development to disease. Circulation. 2012;125:1795–808.
2. Medici D, Kalluri R. Endothelial-mesenchymal transition and its contribution to the emergence of stem cell phenotype. Semin Cancer Biol. 2012;22:379–84.
3. Chen PY, Qin L, Baeyens N, Li G, Afolabi T, Budatha M, et al. Endothelial-to-mesenchymal transition drives atherosclerosis progression. J Clin Invest. 2015;125:4514–28.
4. Magrini E, Villa A, Angiolini F, Doni A, Mazzarol G, Rudini N, et al. Endothelial deficiency of L1 reduces tumor angiogenesis and promotes vessel normalization. J Clin Invest. 2014;124:4335–50.
5. Potenta S, Zeisberg E, Kalluri R. The role of endothelial-to-mesenchymal transition in cancer progression. Br J Cancer. 2008;99:1375–9.
6. Cooley BC, Nevado J, Mellad J, Yang D, St HC, Negro A, et al. TGF-beta signaling mediates endothelial-to-mesenchymal transition (EndMT) during vein graft remodeling. Sci Transl Med. 2014;6:227r–34r.
7. Zhou X, Chen X, Cai JJ, Chen LZ, Gong YS, Wang LX, et al. Relaxin inhibits cardiac fibrosis and endothelial-mesenchymal transition via the Notch pathway. Drug Des Dev Ther. 2015;9:4599–611.
8. Zeisberg EM, Potenta SE, Sugimoto H, Zeisberg M, Kalluri R. Fibroblasts in kidney fibrosis emerge via endothelial-to-mesenchymal transition. J Am Soc Nephrol. 2008;19:2282–7.
9. Hashimoto N, Phan SH, Imaizumi K, Matsuo M, Nakashima H, Kawabe T, et al. Endothelial-mesenchymal transition in bleomycin-induced pulmonary fibrosis. Am J Respir Cell Mol Biol. 2010;43:161–72.
10. Stenmark KR, Frid M, Perros F. Endothelial-to-mesenchymal transition: an evolving paradigm and a promising therapeutic target in PAH. Circulation. 2016;133:1734–7.
11. Reynolds AM, Holmes MD, Danilov SM, Reynolds PN. Targeted gene delivery of BMPR2 attenuates pulmonary hypertension. Eur Respir J. 2012;39:329–43.
12. Sakao S, Hao H, Tanabe N, Kasahara Y, Kurosu K, Tatsumi K. Endothelial-like cells in chronic thromboembolic pulmonary hypertension: crosstalk with myofibroblast-like cells. Respir Res. 2011;12:109.
13. Yang JM, Zhou R, Zhang M, Tan HR, Yu JQ. Betaine attenuates monocrotaline-induced pulmonary arterial hypertension in rats via inhibiting inflammatory response. Molecules. 2018;23:E1274.
14. Maleszewska M, Moonen JAJ, Huijkman N, et al. IL-1β and TGFβ2 synergistically induce endothelial to mesenchymal transition in an NFκB-dependent manner. Immunobiology 2013;218:443–54.
15. Zhu Y, Liu Y, Qian Y, Dai X, Yang L, Chen J, et al. Antimetastatic effects of Celastrus orbiculatus on human gastric adenocarcinoma by inhibiting epithelial-mesenchymal transition and NF-kappaB/snail signaling pathway. Integr Cancer Ther. 2015;14:271–81.
16. Huang T, Chen Z, Fang L. Curcumin inhibits LPS-induced EMT through down-regulation of NF-kappaB-Snail signaling in breast cancer cells. Oncol Rep. 2013;29:117–24.
17. Yeh SH, Wu DC, Tsai CY, Kuo TJ, Yu WC, Chang YS, et al. Genetic characterization of fas-associated phosphatase-1 as a putative tumor suppressor gene on chromosome 4q21.3 in hepatocellular carcinoma. Clin Cancer Res. 2006;12:1097–108.
18. Revillion F, Puech C, Rabenoelina F, Chalbos D, Peyrat JP, Freiss G. Expression of the putative tumor suppressor gene PTPN13/PTPL1 is an independent prognostic marker for overall survival in breast cancer. Int J Cancer. 2009;124:638–43.
19. Zhu JH, Chen R, Yi W, Cantin GT, Fearns C, Yang Y, et al. Protein tyrosine phosphatase PTPN13 negatively regulates Her2/ErbB2 malignant signaling. Oncogene. 2008;27:2525–31.
20. D'Hondt V, Lacroix-Triki M, Jarlier M, Boissiere-Michot F, Puech C, Coopman P, et al. High PTPN13 expression in high grade serous ovarian carcinoma is associated with a better patient outcome. Oncotarget. 2017;8:95662–73.
21. Bamberg A, Redente EF, Groshong SD, Tuder RM, Cool CD, Keith RC, et al. Protein tyrosine phosphatase-N13 promotes myofibroblast resistance to apoptosis in idiopathic pulmonary fibrosis. Am J Respir Crit Care Med. 2018;198:914–27.
22. Zhan H, Jiang J, Luo C, Sun Q, Ke A, Sun C, et al. Tumour-suppressive role of PTPN13 in hepatocellular carcinoma and its clinical significance. Tumour Biol. 2016;37:9691–8.
23. Hopper RK, Moonen JR, Diebold I, Cao A, Rhodes CJ, Tojais NF, et al. In pulmonary arterial hypertension, reduced BMPR2 promotes endothelial-to-mesenchymal transition via HMGA1 and its target slug. Circulation. 2016;133:1783–94.
24. Wang Z, Yang X, Chen L, Zhi X, Lu H, Ning Y, et al. Upregulation of hydroxysteroid sulfotransferase 2B1b promotes hepatic oval cell proliferation by modulating oxysterol-induced LXR activation in a mouse model of liver injury. Arch Toxicol. 2017;91:271–87.
25. Yang J, Dou Z, Peng X, Wang H, Shen T, Liu J, et al. Transcriptomics and proteomics analyses of anti-cancer mechanisms of TR35-An active fraction from Xinjiang Bactrian camel milk in esophageal carcinoma cell. Clin Nutr. 2019;38:2349–59.
26. Maekawa K, Imagawa N, Naito A, Harada S, Yoshie O, Takagi S. Association of protein-tyrosine phosphatase PTP-BAS with the transcription-factor-inhibitory protein IkappaBalpha through interaction between the PDZ1 domain and ankyrin repeats. Biochem J. 1999;337(Pt 2):179–84.
27. Kuo YL, Jou IM, Jeng SF, Chu CH, Huang JS, Hsu TI, et al. Hypoxia-induced epithelial-mesenchymal transition and fibrosis for the development of breast capsular contracture. Sci Rep. 2019;9:10269.
28. Lei R, Zhang S, Wang Y, Dai S, Sun J, Zhu C. Metformin inhibits epithelial-to-mesenchymal transition of keloid fibroblasts via the HIF-1alpha/PKM2 signaling pathway. Int J Med Sci. 2019;16:960–6.
29. Liu L, Chen J, Sun L, Xu Y. RhoJ promotes hypoxia induced endothelial-to-mesenchymal transition by activating WDR5 expression. J Cell Biochem. 2018;119:3384–93.
30. Liu C, Zhou X, Lu J, Zhu L, Li M. Autophagy mediates 2-methoxyestradiol-inhibited scleroderma collagen synthesis and endothelial-to-mesenchymal transition induced by hypoxia. Rheumatology (Oxf). 2019;58:1966–75.
31. Choi SH, Hong ZY, Nam JK, Lee HJ, Jang J, Yoo RJ, et al. A hypoxia-induced vascular endothelial-to-mesenchymal transition in development of radiation-induced pulmonary fibrosis. Clin Cancer Res. 2015;21:3716–26.
32. Ranchoux B, Antigny F, Rucker-Martin C, Hautefort A, Pechoux C, Bogaard HJ, et al. Endothelial-to-mesenchymal transition in pulmonary hypertension. Circulation. 2015;131:1006–18.
33. Good RB, Gilbane AJ, Trinder SL, Denton CP, Coghlan G, Abraham DJ, et al. Endothelial to mesenchymal transition contributes to endothelial dysfunction in pulmonary arterial hypertension. Am J Pathol. 2015;185:1850–8.
34. Romero LI, Zhang DN, Herron GS, Karasek MA. Interleukin-1 induces major phenotypic changes in human skin microvascular endothelial cells. J Cell Physiol. 1997;173:84–92.
35. Lee JG, Ko MK, Kay EP. Endothelial mesenchymal transformation mediated by IL-1beta-induced FGF-2 in corneal endothelial cells. Exp Eye Res. 2012;95:35–9.
36. Chaudhuri V, Zhou L, Karasek M. Inflammatory cytokines induce the transformation of human dermal microvascular endothelial cells into myofibroblasts: a potential role in skin fibrogenesis. J Cutan Pathol. 2007;34:146–53.
37. Mali AV, Joshi AA, Hegde MV, Kadam SS. Enterolactone modulates the ERK/NF-kappaB/Snail signaling pathway in triple-negative breast cancer cell line MDA-MB-231 to revert the TGF-beta-induced epithelial-mesenchymal transition. Cancer Biol Med. 2018;15:137–56.
38. Tong J, Shen Y, Zhang Z, Hu Y, Zhang X, Han L. Apigenin inhibits epithelial-mesenchymal transition of human colon cancer cells through NF-kappaB/Snail signaling pathway. Biosci Rep. 2019;39:BSR20190452.
39. Pahl HL. Activators and target genes of Rel/NF-kappaB transcription factors. Oncogene 1999;18:6853–66.
40. Perkins ND, Gilmore TD. Good cop, bad cop: the different faces of NF-kappaB. Cell Death Differ. 2006;13:759–72.

41. Abaan OD, Levenson A, Khan O, Furth PA, Uren A, Toretsky JA. PTPL1 is a direct transcriptional target of EWS-FLI1 and modulates Ewing's Sarcoma tumorigenesis. Oncogene 2005;24:2715–22.
42. Dromard M, Bompard G, Glondu-Lassis M, Puech C, Chalbos D, Freiss G. The putative tumor suppressor gene PTPN13/PTPL1 induces apoptosis through insulin receptor substrate-1 dephosphorylation. Cancer Res. 2007;67:6806–13.
43. Irie S, Hachiya T, Rabizadeh S, Maruyama W, Mukai J, Li Y, et al. Functional interaction of Fas-associated phosphatase-1 (FAP-1) with p75(NTR) and their effect on NF-kappaB activation. FEBS Lett. 1999;460:191–8.
44. Wang Y, Li M, Huang T, Li J. Protein tyrosine phosphatase L1 inhibits high-grade serous ovarian carcinoma progression by targeting IkappaBalpha. Onco Targets Ther. 2018;11:7603–12.
45. Humbert M, Monti G, Brenot F, Sitbon O, Portier A, Grangeot-Keros L, et al. Increased interleukin-1 and interleukin-6 serum concentrations in severe primary pulmonary hypertension. Am J Respir Crit Care Med. 1995;151:1628–31.
46. Soon E, Holmes AM, Treacy CM, Doughty NJ, Southgate L, Machado RD, et al. Elevated levels of inflammatory cytokines predict survival in idiopathic and familial pulmonary arterial hypertension. Circulation. 2010;122:920–7.
47. Cracowski JL, Chabot F, Labarere J, Faure P, Degano B, Schwebel C, et al. Proinflammatory cytokine levels are linked to death in pulmonary arterial hypertension. Eur Respir J. 2014;43:915–7.
48. Adesina SE, Wade BE, Bijli KM, Kang BY, Williams CR, Ma J, et al. Hypoxia inhibits expression and function of mitochondrial thioredoxin 2 to promote pulmonary hypertension. Am J Physiol Lung Cell Mol Physiol. 2017;312:L599–608.
49. Kojonazarov B, Hadzic S, Ghofrani HA, Grimminger F, Seeger W, Weissmann N, et al. Severe emphysema in the SU5416/hypoxia rat model of pulmonary hypertension. Am J Respir Crit Care Med. 2019;200:515–8.
50. Bowler E, Porazinski S, Uzor S, Thibault P, Durand M, Lapointe E, et al. Hypoxia leads to significant changes in alternative splicing and elevated expression of CLK splice factor kinases in PC3 prostate cancer cells. BMC Cancer. 2018;18:355.